Characterization of partially Ni substituted manganese hexacyanoferrate cathode material

Characterization of partially Ni substituted manganese hexacyanoferrate cathode material

Mariam Maisuradze[a], Min Li[a], Giuliana Aquilanti[b], Jasper Plaisier[b] Marco Giorgetti[a]

[a]Department of Industrial Chemistry "Toso Montanari", University of Bologna, Viale Risorgimento 4, 40136 Bologna, Italy;

[b]Elettra Sincrotrone Trieste, ss 14, km 163.5, 34149, Basovizza, Trieste, Italy

* Correspondence: marco.giorgetti@unibo.it.

Abstract

Manganese Hexacyanoferrate (MnHCF) and partially nickel substituted MnHCF were synthesized by simple co-precipitation method. The water content and chemical formula were obtained by TGA and MP-AES measurements, functional groups by FT-IR analysis, the crystal structure by PXRD and a local geometry by XAS-EXAFS spectroscopy. With the addition of nickel, vacancies and water content increased inside the sample. Crystal structure has changed from monoclinic to cubic. Ni disturbed the local structure of Mn, site, however, almost no change was observed in Fe site.

Keywords

Manganese hexacyanoferrate, X-ray absorption, X-ray diffraction, Cathode Material

1. Introduction

During the battery lifetime, positive and negative electrode materials undergo a continuously reversible redox reaction, and therefore they should be able to allow the rapid insertion and extraction of the ions with the lowest possible lattice strain [1]. In this regard, Prussian Blue (PB) and its analogues (PBAs) (figure S1) are one of the most perspective classes of materials for the cathode development, as they are safe and relatively inexpensive. PBAs are a large family of transition metal hexacyanoferrates ($A_xM[Fe(CN)_6]_{\gamma}\square_{1-\gamma}\cdot zH_2O$, where A is an alkali metal ion, M is transition metal ion and □ is a vacancy; $0<x<2$; $0<y<1$), with open framework structure, redox-active sites and strong structural stability. The

presence of large ionic sites allows the reversible accommodation and easy transfer of the large cations [2]. Among the simple PBAs, MnHCF displays a high specific capacity and redox plateaus at a high voltage [3]. Our group has already studied the electrochemical and structural properties in previous works [3,4]. Metal doping is also widely applied to improve the performance of MnHCF cathode. For example, Ni-doping is used for solving the crystal Jahn-Teller distortion effect in MnHCF, affecting its long-term cycling capability. The atomic radius of Mn is almost equal to the atomic radius of Ni, therefore, during the substitution of manganese with nickel inside the structure, the cubic framework remains in the good order [5].

A number of the conventional laboratory and synchrotron techniques have been used to characterize MnHCF and partially Ni substituted MnHCF materials. Elemental composition was obtained from MP-AES (microwave-plasma atomic emission spectroscopy) and TGA (thermogravimetric analysis) experiments; for structural analysis infra-red spectroscopy (IR), synchrotron-based powder X-ray diffraction (PXRD) and X-ray absorption spectroscopy (XAS) were performed.

2. Experimental

Synthesis was conducted by co-precipitation method, using a process protocol previously established in our group [3], and modified for the nickel addition. $NiSO_4$ was preliminary mixed with $MnSO_4$, in 10/90 or 30/70 ratios for 10% and 30% concentrations of nickel, respectively.

MP-AES analysis was performed by means of MP-AES 4210 high sensitivity optical emission spectrometer. TGA was carried out in TA Discovery TGA instrument. IR spectroscopy was performed by using Bruker Alpha FT-IR spectrometer in attenuated total reflectance (ATR) mode.

XAS experiments were conducted at Sincrotrone Elettra, Basovizza, Italy, at XAFS beamline, in transition mode. The K-edges of Mn, Fe and Ni were collected on the energy range of 6345-7100 eV, 6916 – 8101eV, 8138 – 9567 eV, respectively [6]. XAS spectra were calibrated using the Athena software [7].

PXRD data were recorded at the MCX beamline at Sincrotrone Elettra, Basovizza, Italy. A monochromatic 1 Å X-ray beam was used in a capillary geometry, the spinner at 300 rpm. The crystal structure was refined by GSAS II [8].

3. Results and Discussion

3.1. Formula determination

From the MP-AES and TGA analysis the following formulas were obtained: pure MnHCF - $Na_{1.99}Mn[Fe(CN)_6]_{0.91}\cdot 1.57H_2O$; for 10% Ni-substituted MnHCF - $Na_{1.09}Ni_{0.10}Mn_{0.90}[Fe(CN)_6]_{0.76}\cdot 2.04H_2O$; for 30% Ni-substituted MnHCF - $Na_{1.52}Ni_{0.32}Mn_{0.68}[Fe(CN)_6]_{0.76}\cdot 2.15H_2O$ (Table S1). Generally, it is known that in MnHCF loses absorbed and interstitial water up to 120 °C and 190 °C, respectively. On higher temperature the decomposition of the MnHCF framework occurs [9]. In our material (figure S2), interstitial water loss for MnHCF takes place at 199°C, and Ni addition further shifts it towards the higher temperature, up to 210-218 °C, with addition of 10 and 30% of nickel, respectively.

3.2. IR analysis

On IR spectra (figure 1.a) the signal of C≡N stretching of pure MnHCF is observed at 2066 cm^{-1}, whereas for the partially nickel substituted ones the signal is around 10 cm^{-1} blue shifted. The C≡N band position suggests the domination of the Fe^{II} inside the complex. The shift appearing after the addition of Ni might be ascribed to an increase in the effective charge on the iron-site, weakening the metal−C≡N π back-bonding and strengthening the σ-bonding. The sharp absorptions at 3533 and 1620 cm^{-1} are associated to the O−H stretching and H−O−H bending modes, arising from the interstitial water. While the peak at 3604 cm^{-1} is characteristic to the free surface water (non-hydrogen bonded) [10], a shift of about 13 cm^{-1} was observed for Ni-substituted samples.

3.3. PXRD analysis

The PXRD pattern of the pure MnHCF sample differs from those of containing nickel. On the other hand, partially Ni substituted samples have quite similar PXRD data, but there is a shift towards the higher angles with the increase of nickel concentration (figure 1.b).

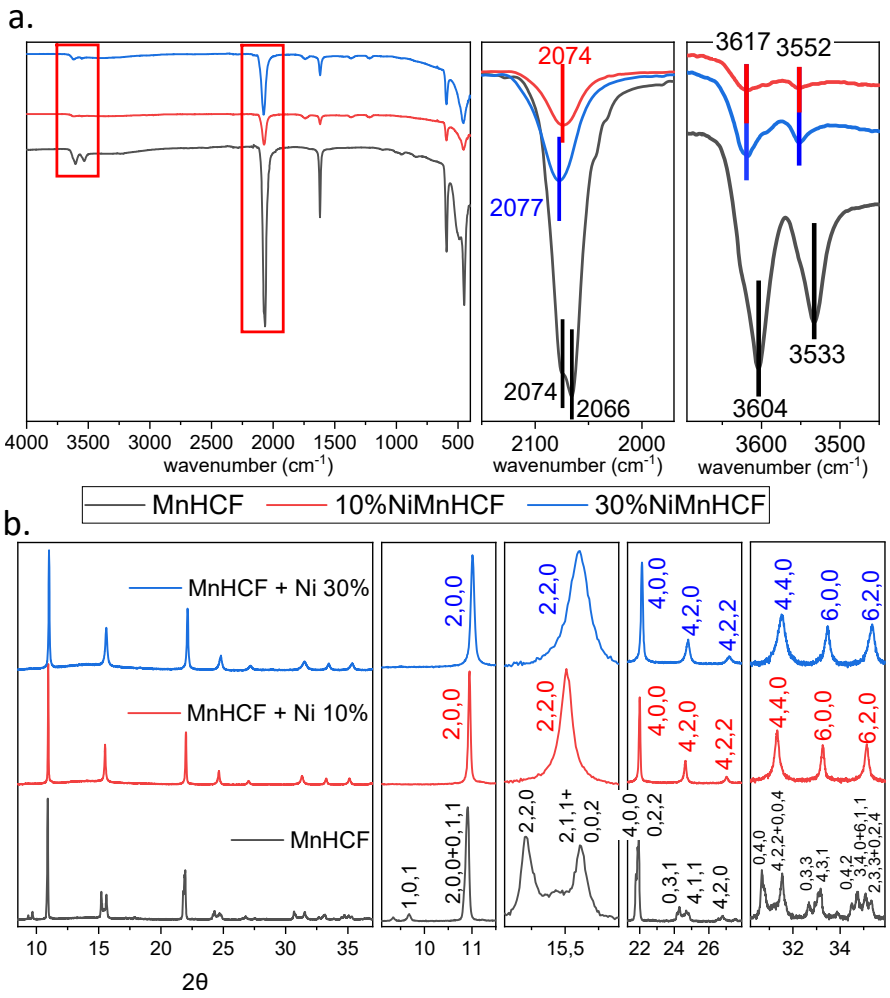

Figure 1. MnHCF (black), MnHCF + Ni 10% (red) and MnHCF + Ni 30% (blue): IR spectra (a) and PXRD (b).

For the assignment of the crystal structure Rietveld refinement was conducted (Table S2). The space group of the pure MnHCF was refined to the monoclinic structure, P 21/n (figure 2.a), as expected [3]. However, Ni-doping altered the crystal structure, an attempt of refining the structure with a P 21/n model has failed due to the existence of the obvious higher symmetric structure. The structure was therefore refined to cubic, Fm-3m (figure 2.b, c), using a structural model based on neutron diffraction data of $K_{2x/3}Cu[Fe(CN)_6]_{2/3}\cdot nH_2O$ [11]. Nickel was refined on the same atomic position as manganese. Both substituted samples appear to have a very similar structure, with the small decrease of the cell

volume for 30% Ni.

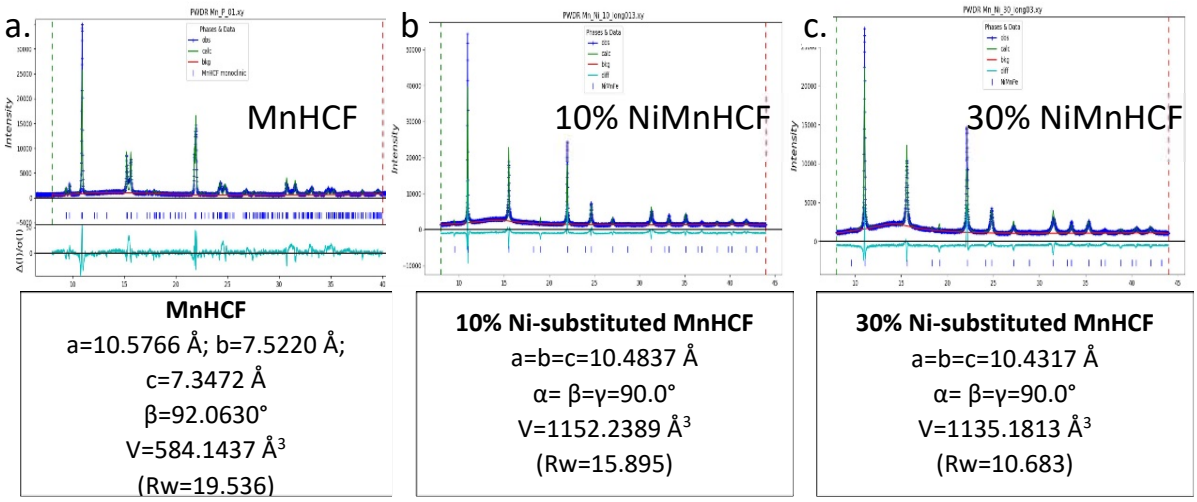

Figure 2. Rietveld refinement results obtained from GSAS II software of MnHCF (a), 10% Ni-substituted MnHCF (b) and 30% Ni-substituted MnHCF (c).

3.4. XANES analysis

Iron is bound to σ-donor and π-acceptor carbon and therefore experiences the strong crystal field, leading to a low spin (LS) state, with $t_{2g}^6 e_g^0$ electron configuration, octahedral environment (figure 4.d). In Fe pre-edge region (figure 4.a) a single transition at around 7113-7114 eV can be assigned to the dipole forbidden, quadrupole allowed transition 1s→3d e_g [12]. Transitions occurring at higher energies of the pre-edge region (>7115 eV), arise from forbidden dipole transitions to the empty bound states [13]. The only difference between pure and partially Ni-substituted sample in the pre-edge part is the disappearance of the low intensity transition at 7123.2 eV. The edge is quite similar in all samples, centred at ≈7130 eV. It can be concluded, that the second metal addition has not influenced the oxidation state of Fe.

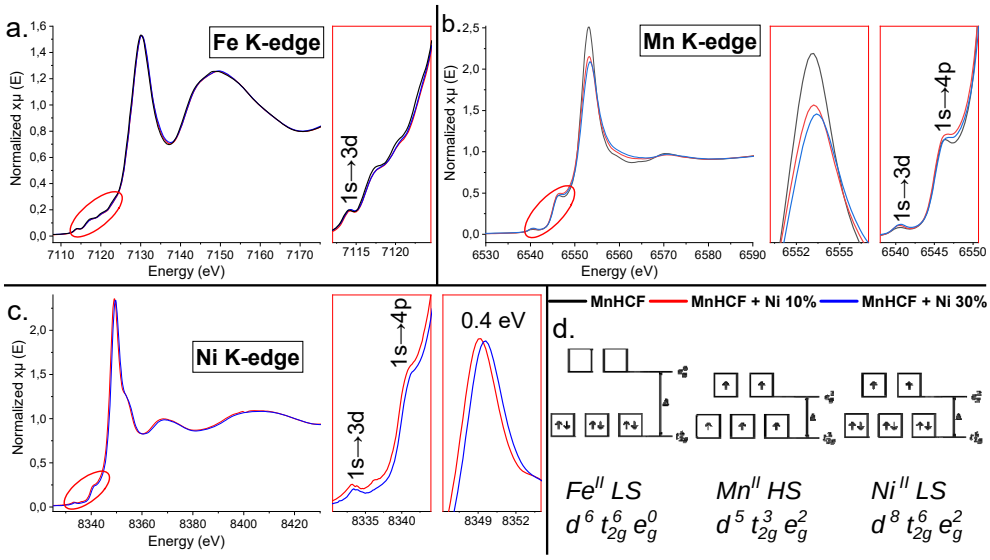

Figure 3. XANES K-edge of: Fe with the zoom at pre -edge (a); Mn with the zoom at the edge and pre-edge (b); Ni K with the zoom at the edge and pre-edge (c); and electronic configurations of the 3d orbitals of Fe^{II}, LS; Mn^{II}, HS and Ni^{II} 3d, HS in the octahedral environment (d).

Manganese is bounded to N-end of the cyanide ligand, experiencing a moderate crystal field, as nitrogen is σ-donor. Consequently, Mn is in the high spin (HS) state Mn^{II}, $3d^5$ ($t_{2g}^3 + e_g^2$), also having an octahedral environment [14], d^5 configuration (figure 3.d). In the pre-edge region, the transitions 1s→3d t_{2g}/e_g at ≈6540 eV and 1s→4p at ≈6546 eV (figure 3.b) can be observed. Edge is centred at ≈ 6553.2 eV, except 30% Ni- substituted sample, which is slightly shifter towards the higher energy: ≈ 6553.4 eV. More significant changes are observed in absorption intensity - the addition of nickel decreases the intensity, which is logical as Ni substitutes the manganese inside the structure, also suggested by PXRD data refinement. XANES results of iron and manganese K-edges are in a good agreement with the previously published results from Mullaliu et al. [3].

Pre-edge transitions and edge energy of nickel suggests HS Ni^{2+}, d^8 configuration, octahedral environment (figure 3.d), which again points to six cyanide ligands coordinating from the N-end and therefore the partial substitution of Mn with Ni inside the structure. In the pre-edge region 1s→3d at ≈8333 eV and 1s→4p peak at ≈8341 eV transitions are observed. 10% Ni- substituted MnHCF has small shift towards the lower energy of 0.2 eV for 1s→3d, 0.6 eV and 1s→4p transitions and 0.4 eV for the edge energy compare to 30% Ni (figure 3.c), which suggests the decrease of the oxidation state.

3.5. EXAFS fitting

EXAFS gives a relevant structural information of the local coordination site around the metals. A multiple-edge fitting analysis have been conducted simultaneously at the Fe, Mn and Ni K-edge using the GNXAS program [15], using the prescription for a correct extraction and interpretation of the EXAFS spectrum in this class of samples, reported recently [16]. Figure 4 displays the EXAFS Multiple edge refinement of the 10% Ni- substituted MnHCF sample at the three considered metal edges and the fitting results are summarized in Table S2. The bond lengths of Fe-C and C≡N are kept almost same. Consequently, the local structure around the iron-site is not disturbed. On the other hand, the bond length Mn-N is gradually reducing, from 2.18 to 2.15, and 2.12 Å with the increase of Ni content. Corresponding Debye-Waller factors confirm that Mn site gets more distorted. The Ni replaced the Mn in the structure, with shorter Ni-N first shell interaction, at 2.06 Å.

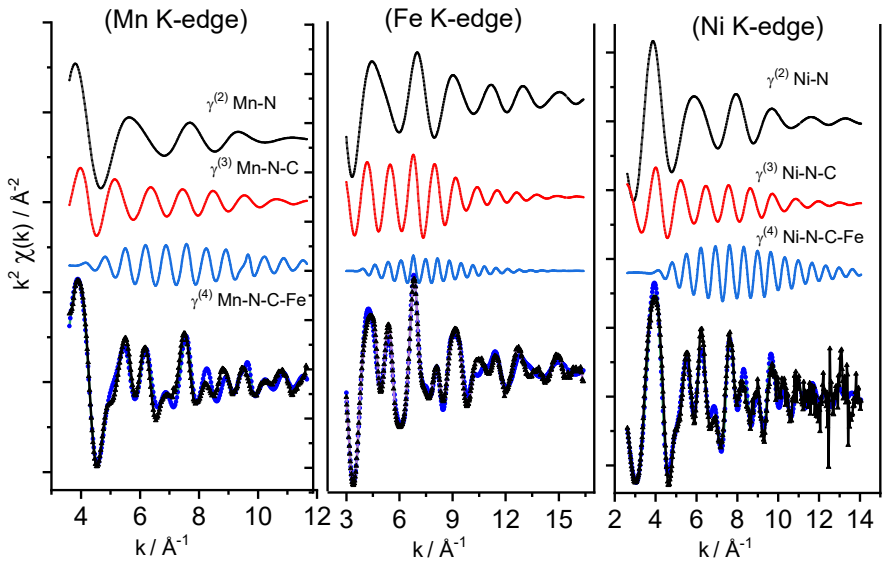

Figure 4. EXAFS Multiple edge refinement of the 10% Ni- substituted MnHCF.

4. Conclusion

The addition of nickel to MnHCF has caused the increase of both vacancies and water content inside the material. PXRD showed the increase of symmetry from monoclinic P 21/n to cubic F m-3m. Both PXRD and XAS analysis suggested that Ni occupies the same position as Mn and from EXAFS fitting local structure disturbance at Mn site was observed. Interestingly, according to XANES analysis varying Ni content from 10 to 30% triggered the increase in oxidation state of nickel and manganese-sites.

References

[1] J.-M. Tarascon, et al., Nature. 414 (2001) 359–367. https://doi.org/10.1038/35104644.

[2] J. Qian, et al., Advanced Energy Materials. 8 (2018) 1702619. https://doi.org/10.1002/aenm.201702619.

[3] A. Mullaliu, et al., Small Methods. 4 (2020) 1900529. https://doi.org/10.1002/smtd.201900529.

[4] M. Li, R et al., Electrochimica Acta. 400 (2021) 139414. https://doi.org/10.1016/j.electacta.2021.139414.

[5] D. Yang, et al., Chem. Commun. 50 (2014) 13377–13380. https://doi.org/10.1039/C4CC05830E.

[6] G. Aquilanti, et al., Journal of Physics D: Applied Physics. 50 (2017) 074001. https://doi.org/10.1088/1361-6463/aa519a.

[7] B. Ravel, et al., Journal of Synchrotron Radiation. 12 (2005) 537–541. https://doi.org/10.1107/S0909049505012719.

[8] B.H. Toby, et al., Journal of Applied Crystallography. 46 (2013) 544–549. https://doi.org/10.1107/S0021889813003531.

[9] J. Song, et al., J Am Chem Soc. 137 (2015) 2658–2664. https://doi.org/10.1021/ja512383b.

[10] P.J. Kulesza, et al., Analytical Chemistry. 6 (1996) 2442–2446. https://doi.org/10.1021/ac950380k.

[11] D. Wardecki, et al., Crystal Growth & Design. 17 (2017) 1285–1292. https://doi.org/10.1021/acs.cgd.6b01684.

[12] A. Mullaliu, et al., Condensed Matter. 3 (2018) 36. https://doi.org/10.3390/condmat3040036.

[13] N. Kosugi, et al., Chemical Physics. 104 (1986) 449–453. https://doi.org/10.1016/0301-0104(86)85034-0.

[14] M.-A. Arrio, et al., J Am Chem Soc. 118 (1996) 6422–6427. https://doi.org/10.1021/ja9542698.

[15] A. Filipponi, et al., Physical Review B. 52 (1995) 15122–15134. https://doi.org/10.1103/PhysRevB.52.15122.

[16] M. Giorgetti, et al., Multi-edge and Multiple Scattering EXAFS Analysis of Metal Hexacyanoferrates: Application in Battery Materials, in: 2021: pp. 99–109. https://doi.org/10.1007/978-3-030-72005-6_8.

Acknowledgements

Measurements at ELETTRA were supported by in-house research. This research was funded by the University of Bologna, RFO funding. M. Maisuradze acknowledges the support of CERIC-ERIC for providing the PhD bourse.